# Positive feedbacks between the Antarctic Circumpolar Wave and the global El Niño-Southern Oscillation Wave

Warren B. White and Shyh-Chin Chen
Scripps Institution of Oceanography, La Jolla, California, USA

Rob J. Allan[1]
CSIRO Atmospheric Research, Aspendale, Victoria, Australia

Roger C. Stone
Department of Primary Industries, Toowoomba, Queensland, Australia

Received 1 August 2000; revised 9 October 2001; accepted 5 November 2001; published 19 October 2002.

[1] Atmospheric and oceanic teleconnections link the Antarctic Circumpolar Wave (ACW) in the Southern Ocean [*White and Peterson*, 1996] and the global El Niño-Southern Oscillation (ENSO) wave (GEW) in the tropical Indo-Pacific Ocean [*White and Cayan*, 2000], both signals characterized by eastward phase propagation and 3- to 5-year-period variability. We extend the tropical standing mode of ENSO into the extratropics by regressing the Niño-3 sea surface temperature (SST) index against sea level pressure (SLP) anomalies over the globe, finding the Pacific-South America (PSA) pattern in SLP anomaly [*Cai and Baines*, 2001] straddling Drake Passage in the Southern Ocean. The amplitude of this PSA pattern is ~1/3 that of the ACW in this domain and thus cannot be considered its principal driver. On the other hand, suppressing the tropical standing mode of ENSO in interannual ST (surface temperature) and SLP anomalies over the globe allows the GEW to be observed much more readily, whereupon its eastward phase propagation across the Warm Pool is found to remotely force the ACW in the eastern Pacific and western Atlantic sectors of the Southern Ocean through atmospheric teleconnections [*Sardeshmukh and Hoskins*, 1988] which propagate along with it. Subsequently, the ACW propagates this imposed GEW signal throughout the remainder of the Southern Ocean as a coupled wave in covarying ST and SLP anomalies, whereupon entering the Indian sector 1.5 to 2.5 years later it spawns a northern branch which takes another 1.5 to 2.5 years to propagate the ACW signal equatorward into the Warm Pool south of Indonesia. There it interferes constructively with the GEW. Thus the two forms of teleconnection, one fast and directed from the tropics to the high southern latitudes via the atmosphere and the other slow and directed from the high southern latitudes to the tropics via the ocean, complete a global circuit of 3- to 5-year duration that reinforces both the ACW and GEW and influences the tropical standing mode of ENSO. *INDEX TERMS:* 4207 Oceanography: General: Arctic and Antarctic oceanography; 4215 Oceanography: General: Climate and interannual variability (3309); 4522 Oceanography: Physical: El Niño; 4504 Oceanography: Physical: Air/sea interactions (0312); 3339 Meteorology and Atmospheric Dynamics: Ocean/atmosphere interactions (0312, 4504); *KEYWORDS:* ACW, ENSO, teleconnections, ocean-atmosphere coupling

**Citation:** White, W. B., S.-C. Chen, R. J. Allan, and R. C. Stone, Positive feedbacks between the Antarctic Circumpolar Wave and the global El Niño–Southern Oscillation Wave, *J. Geophys. Res.*, *107*(C10), 3165, doi:10.1029/2000JC000581, 2002.

## 1. Introduction

[2] Recent observations of the El Niño-Southern Oscillation (ENSO) of 3- to 5-year period scale in global surface temperature (ST) and sea level pressure (SLP) data sets finds the tropical standing mode of ENSO [*Allan*, 2000] superimposed on an eastward propagating global ENSO wave (GEW) [*White and Cayan*, 2000]. This GEW appears to be initiated in the western tropical Indian Ocean by zonal atmospheric teleconnections associated with the tropical standing mode of ENSO [*Tourre and White*, 1997], with covarying ST and SLP anomalies taking 3 to 4 years to propagate eastward across the Indo-Pacific Ocean along the mean path of the Intertropical Convergence Zone (ITCZ),

[1]Now at Hadley Centre for Climate Prediction and Research, Bracknell, UK.


0148-0227/02/2000JC000581

providing a delayed positive feedback to El Niño/La Niña in the eastern equatorial Pacific Ocean [*White and Cayan*, 2000]. Subsequently, the GEW in covarying ST and SLP anomalies takes another 1 to 2 years to propagate from the eastern tropical Pacific Ocean into the eastern tropical Atlantic Ocean via the Caribbean Sea. Thus the GEW transits the global tropical ocean in 4 to 6 years at a zonal average speed of 60° to 90° of longitude per year (i.e., 0.20 to 0.32 m $s^{-1}$).

[3] Contemporaneous with the slow eastward propagation of the GEW across the global tropical ocean is the slow eastward propagation of the ACW across the Southern Ocean in covarying ST and SLP anomalies on the same 3- to 5-year-period scale, taking ~8 years to circle the globe, traveling at a zonal average speed of ~45° longitude per year (i.e., 0.08 m $s^{-1}$) [*White and Peterson*, 1996; *Jacobs and Mitchell*, 1996]. *Qiu and Jin* [1997] found the ACW to be independent of the GEW when viewed in the global average. Indeed, this would seem to be so since the zonal average speed in degrees longitude per year for the ACW is 1/2 to 2/3 that for the GEW. Yet here in the present study we demonstrate that the two traveling wave phenomena are linked but only over selected longitude domains.

[4] Already, the ACW in the eastern Pacific sector of the Southern Ocean has been shown to be influenced by the tropical standing mode of ENSO through two different kinds of meridional teleconnection. *Peterson and White* [1998] examined the slower of the two teleconnections, finding the tropical standing mode of ENSO initiating maximum anomalous Hadley cell activity in the western Pacific Ocean near 180° longitude, the subtropical limb of which generates ST anomalies north of New Zealand during El Niño/La Niña. During the transition between El Niño and La Niña these SST anomalies propagate poleward and eastward together with covarying SLP anomalies into the eastern Pacific sector of the Southern Ocean, where they interfere constructively with covarying ST and SLP anomalies in the ACW. Earlier *Karoly* [1989] examined the faster of the two teleconnections, finding the tropical standing mode of ENSO initiating anomalous Hadley cell activity in the western Pacific Ocean, with anomalous divergence in the subtropical limb initiating quasi-stationary Rossby waves in the mean upper level Westerly Winds. These quasi-stationary Rossby waves allow the tropical standing mode of ENSO to penetrate its influence into the eastern Pacific and western Atlantic sectors of the Southern Ocean along a great circle route extending from the subtropical ocean north of New Zealand through Drake Passage. *Carleton* [1989] also linked ENSO to this standing mode in SLP anomaly straddling Drake Passage, which has come to be known as the Pacific–South America (PSA) pattern. Recently, *Cai and Baines* [2001] proposed that the remotely forced PSA pattern in SLP anomaly acts to pump the ACW in the eastern Pacific and western Atlantic sectors, which during the transition between El Niño and La Niña propagates eastward into the eastern Atlantic, Indian, and western Pacific sectors of the Southern Ocean under its own coupling dynamics [*Baines and Cai*, 2000]. They argued that unless the tropical standing mode of ENSO is robust, the ACW would not be generated.

[5] In the present study we find a different situation. We find the PSA pattern in SLP anomaly too weak to force the ACW in the eastern Pacific and western Atlantic sectors of the Southern Ocean. Instead, we find the ACW propagating eastward across this domain from 150°W to 30°W in fixed phase with the GEW propagating eastward across the tropical Warm Pool from 90°E to 150°W, linked through atmosphere teleconnections traveling with the GEW. The consistent phasing between the GEW and the ACW, and the latter's amplitude growth across the eastern Pacific and western Atlantic sectors, indicate that the ACW is in "damped resonance" with remote forcing by the GEW. On the other hand, once the ACW is amplified in this region, it takes 1.5 to 2.5 years to propagate as a coupled wave in covarying ST and SLP anomaly into the Indian sector of the Southern Ocean. There it spawns an interannual signal in covarying ST and SLP anomalies propagating northward, which takes another 1.5 to 2.5 years to reach the tropical Warm Pool, observed earlier by *Peterson and White* [1998], where it interferes constructively with the GEW. This completes a global circuit of 3- to 5-year duration, which reinforces both the ACW and the GEW, and influences the tropical standing mode of ENSO.

## 2. Data and Methods

[6] We analyze five variables from the National Centers for Environmental Prediction and National Center for Atmospheric Research (NCEP/NCAR) reanalysis [*Kalnay et al.*, 1996]. We analyze monthly ST, SLP, 200-hPa divergence (D200), and 200-hPa divergent zonal and meridional wind components (DU200 and DV200), available monthly on a 2.5° latitude-longitude grid over the globe for 18 years from 1982 to 1999, a period beginning when sea surface temperature (SST) first became available over the global ocean from satellite radiometry [e.g., *Reynolds and Marsico*, 1993]. Over the ocean the NCEP/NCAR reanalysis incorporates the COADS surface marine weather observations [*Slutz et al.*, 1985], the Reynolds' SST analysis [*Reynolds and Marsico*, 1993], and atmospheric soundings from weather ships and satellites [*Kalnay et al.*, 1996]. In the NCEP/NCAR reanalysis, ST over the ocean is SST and over the land it is surface air temperature (SAT).

[7] Monthly anomalies of ST, SLP, D200, DU200, and DV200 were computed about long-term monthly means defining the mean annual cycle over the 18-year record. Zonal wave number-frequency spectra of monthly ST and SLP anomalies along the equator in the Indo-Pacific Ocean [*White and Cayan*, 2000] and along 56°S in the Southern Ocean [*White and Peterson*, 1996] yield peak spectral energy density for interannual signals of 3- to 5-year period. This allows us to isolate interannual signals from higher- and lower-frequency variability by band-pass filtering using a period admittance window with half power points at 3 and 7 years [*Kaylor*, 1977]. To reduce loss of data at both ends of each time sequence due to high-pass filtering, maximum entropy spectral analysis was applied [*Andersen*, 1974] using spectral coefficients to extend the time sequences by an amount equal to half the filter width; this procedure retains 1/2 of the interannual signal on average at both ends of the record [*White*, 2001]. For the 18-year record, band-pass filtering yields approximately five cycles of interannual variability with ~10 effective temporal degrees of freedom

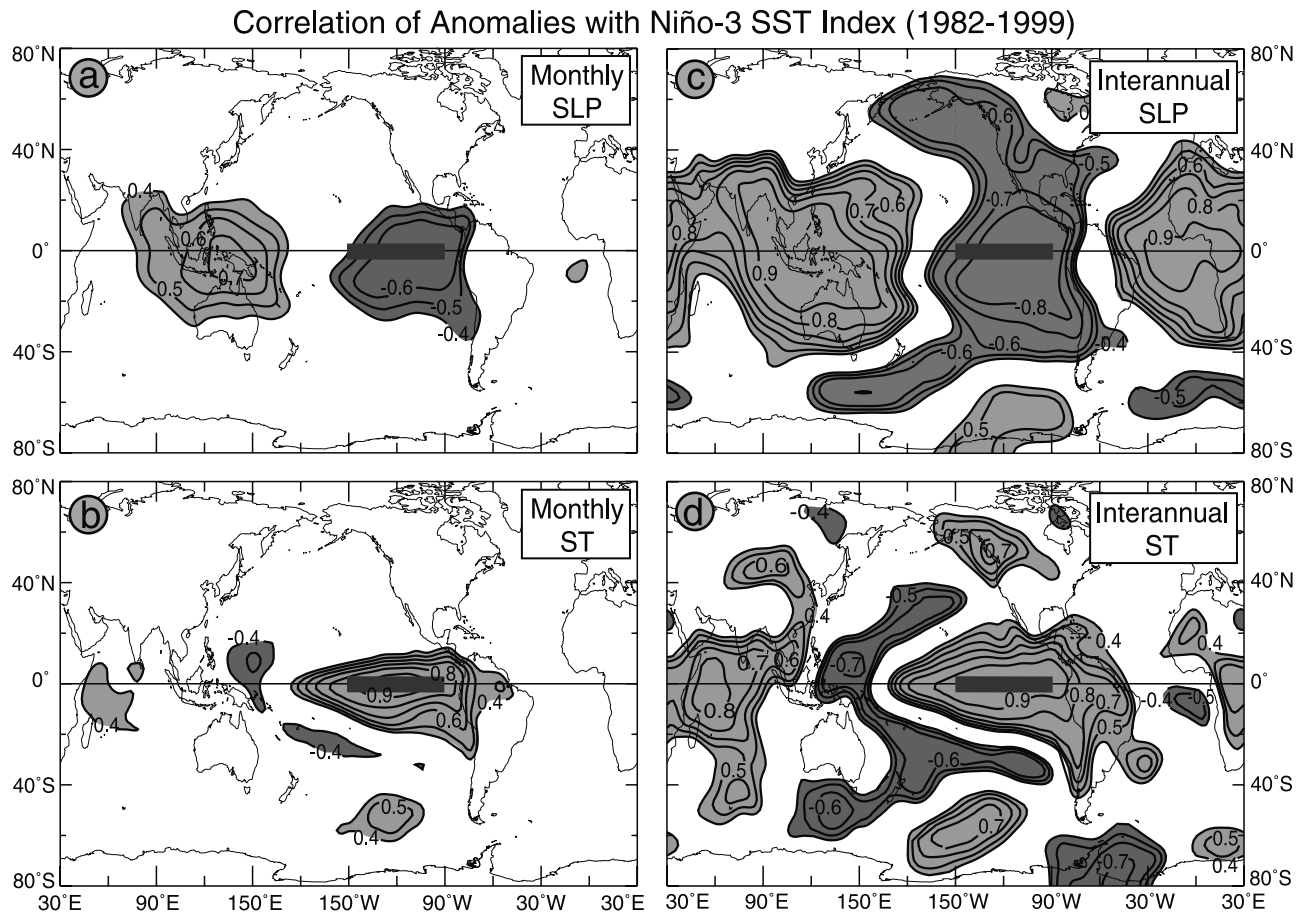


**Figure 1.** (a) The global distribution of correlation between the monthly Niño-3 SST index and monthly SLP anomalies over the rest of the globe from 80°S to 80°N for the 18 years from 1982 to 1999. (b) Same as in Figure 1a but for the monthly Niño-3 SST index and monthly ST anomalies over the rest of the globe. (c) The global distribution of correlation between the interannual Niño-3 SST index and interannual SLP anomalies over the rest of the globe. (d) Same as in Figure 1c but for the interannual Niño-3 SST index and interannual ST anomalies over the rest of the globe. Only correlations greater than 0.4 are displayed, as only those greater than 0.54 are significant at the 90% confidence level given ~10 effective degrees of freedom [*Snedecor and Cochran*, 1980]. Positive (negative) correlations are shaded dark (light) for effect. In each distribution the location of the Niño-3 SST index is given by the rectangular shaded box.

[*Snedecor and Cochran*, 1980]. The filtering procedure reduced the standard errors of the anomalies by a factor of 7 or so; that is, the square root of 48 nearly independent monthly estimates in the low-pass portion of the band-pass filter. This means that standard errors for interannual anomalies are approximately ±0.02° for ST and ±0.07 hPa for SLP.

[8] We also utilize modified interannual ST, SLP, D200, DU200, and DV200 anomalies in which the tropical standing mode of ENSO has been suppressed. We accomplish this suppression by regressing the Niño-3 SST index against the five variables over the globe and then subtracting that portion associated with the tropical standing mode of ENSO. The rationale for this procedure derives from *White and Cayan* [2000], who used complex empirical orthogonal function (CEOF) analysis to separate the tropical standing mode of ENSO from the eastward propagating GEW for the 20 years from 1975 to 1994. They found the first CEOF mode accounting for 80% to 90% of the interannual Niño-3 SST index during the 1983 and 1987 El Niño events, with 2/3 of interannual variability explained by the tropical standing mode of ENSO and the other 1/3 explained by the eastward traveling GEW. Thus we subtract 2/3 of the portion of the interannual Niño-3 SST index regressed against the other five variables. This procedure allows the ACW in the Southern Ocean and the GEW in the global tropical ocean to be observed relatively free from contamination by the tropical standing mode of ENSO.

## 3. Extending the Tropical Standing Mode of ENSO to the Globe

[9] We correlate the Niño-3 SST index against SLP and ST anomalies over the globe from 80°S to 80°N for the 18 years from 1982 to 1999 using monthly anomalies (Figures 1a and 1b) and interannual anomalies (Figures 1c and 1d). On monthly period scales this influence is confined mostly to the tropical Pacific Ocean, but on interannual period scales

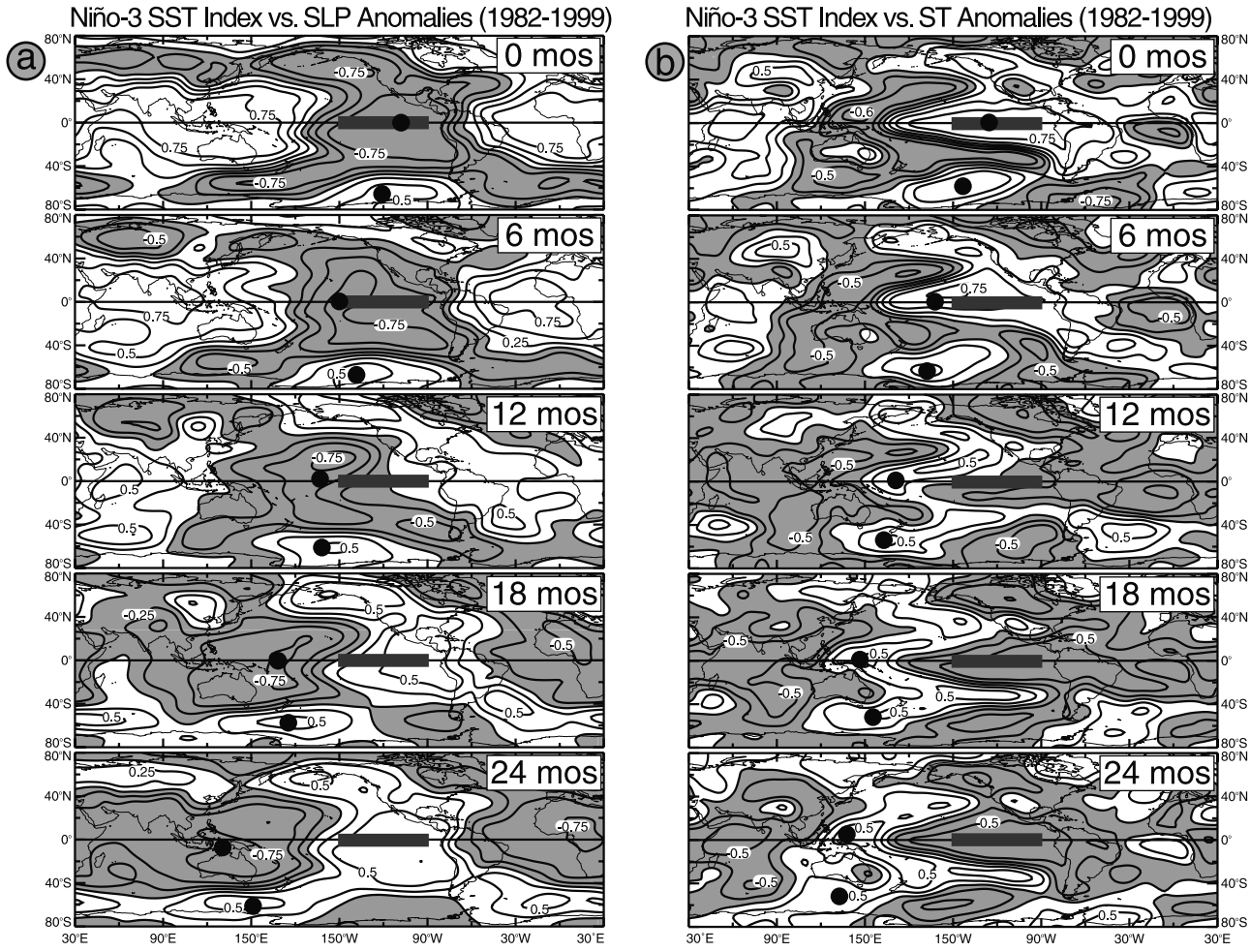


**Figure 2.** (a) The global distribution of correlation between the interannual Niño-3 SST index and interannual SLP anomalies over the rest of the globe from 80°S to 80°N for the 18 years from 1982 to 1999 at lead months of 0, 6, 12, 18, and 24. Positive (negative) correlation coefficients are unshaded (shaded). Only correlations greater than 0.54 are significant at the 90% confidence level given ~10 effective degrees of freedom [*Snedecor and Cochran*, 1980], but large coherent patterns with magnitudes smaller than 0.54 are also significant. (b) Same as in Figure 2a but for the correlation of interannual ST anomalies with the interannual Niño-3 SST index. Propagation can be discerned by following the two solid dots with increasing lag (decreasing lead), one dot associated with correlation patterns on the equator and the other associated with correlation patterns at 56°S. Elsewhere propagation can be discerned by following negative and positive correlation patterns with increasing lag (decreasing lead).

it extends over the entire globe, penetrating south into the Southern Ocean via meridional atmospheric teleconnections and revealing an apparent global standing mode of ENSO. As we shall demonstrate below, the projection of the Niño-3 SST index into the tropical Indian and Atlantic Ocean occurs in response to anomalous Walker cell activity [e.g., *Webster*, 1994], while its extension into the Southern Ocean occurs in response to anomalous Hadley cell activity [*Karoly*, 1989; *Sardeshmukh and Hoskins*, 1988; *Cai and Baines*, 2001], both zonal and meridional cells apparently driven by anomalous SST-induced vertical convection in the tropical Indo-Pacific Ocean [*Graham and Barnett*, 1987] and mediated by divergent wind anomalies at the top of the troposphere near 200 hPa.

[10] Throughout the Southern Ocean, unlike the high-latitude Northern Hemisphere, the interannual Niño-3 SST index correlates with a global zonal wave number two-pattern of variability in both ST and SLP anomalies extending zonally around the Southern Ocean between 40°S and 70°S. Yet only that portion of this ''global'' standing mode of ENSO in the eastern Pacific and western Atlantic sectors of the Southern Ocean can be traced directly to the tropical standing mode of ENSO. The dynamics of this connection was first examined by *Karoly* [1989], and later revised by *Sardeshmukh and Hoskins* [1988], who found quasi-stationary Rossby waves in mean winter upper level Westerly Winds over the eastern Pacific and western Atlantic sectors of the Southern Ocean occurring in response to anomalous 200-hPa divergence in the subtropical limb of the anomalous Hadley Cell in the western tropical Pacific Ocean and to the anomalous advection of absolute vorticity in the mean Westerly Winds east of Australia by meridional divergent winds at 200 hPa. The remaining portion of the ''global'' standing mode of ENSO in the eastern Atlantic, Indian, and

western Pacific sectors of the Southern Ocean arises because the ACW conducts ENSO signals imposed on it in the eastern Pacific and western Atlantic sectors into the remaining sectors over the following 8 years [*Cai and Baines*, 2001]. Thus correlations between the Niño-3 SST index and ST and SLP anomalies in the eastern Atlantic, Indian, and western Pacific sectors of the Southern Ocean do not indicate direct cause and effect via atmosphere teleconnections; rather, a coincidence occurs between the ACW and the tropical standing mode of ENSO over this domain.

[11] In the global distribution of the SLP correlation (Figure 1c) we see the characteristic signature of a quasi-stationary Rossby wave train [*Sardeshmukh and Hoskins*, 1988, Figure 10] following a great circle route extending southeast from the subtropics north of New Zealand near 30°S through Drake Passage, yielding the PSA pattern of standing mode SLP variability [e.g., *Cai and Baines*, 2001]. The anomalous geostrophic wind pattern inferred from this SLP correlation distribution is in phase with the anomalous ST pattern (Figure 1d) with poleward (equatorward) and westward (eastward) surface wind anomalies overlying warm (cool) ST anomalies. This is consistent with anomalous zonal wind-induced processes of latent-plus-sensible heat flux, Ekman meridional heat flux, and/or vertical mixing at the base of the near-surface mixed layer, acting to force the high-latitude standing mode of ST anomaly [*White et al.*, 1998]. As we shall see below, this forcing of ST anomalies in this region by anomalous winds associated with the PSA represents only a portion of the action; the other portion derives from the remote forcing of the ACW by the GEW in this domain.

## 4. Links Between the GEW and the ACW

[12] We correlate the Niño-3 SST index against SLP and ST anomalies over the globe from 80°S to 80°N for the 18 years from 1982 to 1999 for different leads at 0, 6, 12, 18, and 24 months (Figure 2). This allows us to visualize the slow eastward propagation of the GEW in the tropics and of the ACW in the Southern Ocean and their possible interactions. In the Southern Ocean, positive SLP correlations in the eastern Pacific sector west of Drake Passage at lead month 0 (Figure 2a) can be seen displaced sequentially westward to the region south of Australia by lead month 24, a distance of ~90° of longitude in 2 years, occurring at the speed of ~45° longitude per year for the ACW (that is, ~0.08 m $s^{-1}$). Its reverse evolution is accompanied by the westward displacement of negative correlations associated with the GEW in the eastern tropical Pacific Ocean. This correspondence can be discerned by following the two black dots in Figure 2a, one associated with the negative correlation pattern on the equator and the other associated with positive correlation patterns at 56°S. Both tropical and extratropical SLP correlations can be seen displaced westward (eastward) together with increasing lead (lag), representing the eastward phase propagation of SLP anomalies associated with the ACW in the Southern Ocean and associated with that of the GEW across the tropical Pacific Ocean. A similar propagation can be seen in the evolution of positive ST correlations in the eastern tropical Pacific Ocean and the eastern Pacific sector of the Southern Ocean (Figure 2b). This longitudinal correspondence in speed and phase between the GEW and the ACW in the Pacific basin suggest that both are linked through atmosphere teleconnections similar to that observed for the tropical standing mode of ENSO [e.g., *Cai and Baines*, 2001].

[13] On the other hand, examining the evolution of positive SLP correlations in the middle of the Warm Pool near Indonesia at lead month 0 reveals a different picture (Figure 2a). For increasing lead we find these SLP correlations sequentially displaced westward to the east coast of Africa and southward into the Indian sector of the Southern Ocean over the lead months 6, 12, and 18. A similar evolution can be seen in the negative ST correlations in the Warm Pool near Indonesia at lead month 0 (Figure 2b). This is consistent with the GEW taking 18 to 24 months to propagate slowly eastward across the tropical Indian Ocean with increasing lag [*Tourre and White*, 1997; *White and Cayan*, 2000], and it is indicative of the north branch of the ACW also taking 18 to 24 months to propagate slowly northeastward across the Indian Ocean from high latitude to the tropics [*Peterson and White*, 1998]. Thus both the ACW and the GEW in the Indian Ocean can be seen influencing SLP anomalies in the Warm Pool, interfering constructively to maintain the interannual signal there. Since covarying ST and SLP signals in the Warm Pool affect the Niño-3 SST index 18 to 24 months later, the confluence of signals from the ACW with those of the GEW in the Warm Pool also affect the amplitude and phase of the tropical standing mode of ENSO.

## 5. Links Between the GEW and the ACW in the Absence of the Tropical Standing Mode of ENSO

[14] We display animation sequences of modified interannual SLP and ST anomalies (see section 2) from 20°N to 70°S for 10 years from January 1983 to January 1993 (Figure 3), wherein the ACW in the Southern Ocean and the GEW in the global tropical ocean to be observed relatively free from contamination by the tropical standing mode of ENSO. For example, the ACW can be seen propagating eastward in high SLP (warm SST) anomalies in the Southern Ocean, beginning south of Africa in June 1985 (June 1986) and ending in Drake Passage in January 1992 (January 1993). As well, the GEW can be seen propagating eastward in high SLP and cool SST anomalies in the global tropical ocean, beginning southeast of India in January 1986, crossing the Warm Pool, and ending in the central equatorial Pacific Ocean in January 1989.

[15] As indicated in Figure 2, we can now observe covarying SLP and ST anomalies in the ACW interfering constructively with those in the GEW in the tropical Warm Pool near Indonesia (Figure 3) by following their evolution from 1985 to 1990. We begin with high SLP and warm ST anomalies in the ACW south of Madagascar in 1985 and 1986, respectively, where high SLP anomalies are displaced to the east of warm SST anomalies by ~90° of phase. We find these warm ST anomalies propagating into the central middle latitude Indian Ocean by June 1987, into the west coast of Australia and south of Australia by June 1988, and into the Warm Pool north of Australia (near Indonesia) by January of 1989. By June 1989, warm ST anomalies completely surround Australia. By June 1990 these anomalies propagate eastward along both northern and southern

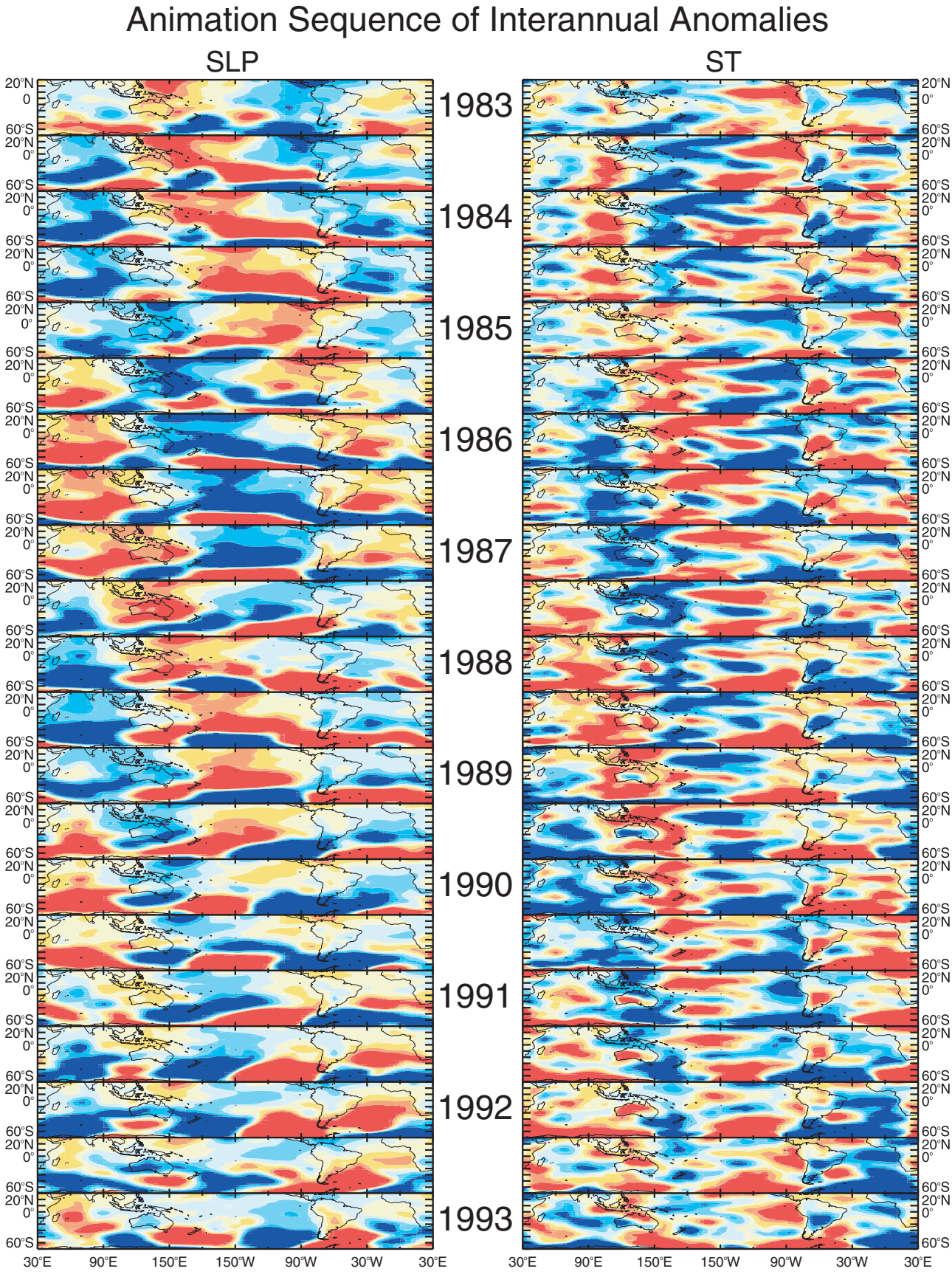

paths, penetrating into the western tropical Pacific Ocean on the north, crossing the Warm Pool from west to east, and surrounding New Zealand on the south. By June 1991 the warm ST anomalies along the northern path propagate eastward into the central equatorial Pacific Ocean and those along the southern path propagate eastward into the Bellingshausen Sea, all the while being led by (underlying) high SLP anomalies in the high latitude (tropics). Thus the ACW in the Indian Ocean can be seen to interfere constructively with the GEW in the Warm Pool near Indonesia, the latter continuing to propagate eastward into the central equatorial Pacific Ocean where it can influence the development of the tropical standing mode of ENSO.

[16] We display time-longitude diagrams of the interannual SLP anomalies along the equator and along 56°S (Figures 4a and 4d), of interannual SLP anomalies with tropical standing mode of ENSO suppressed (Figures 4b and 4e), and the difference between the two, reflecting the tropical standing mode of ENSO on the equator and the PSA pattern at 56°S (Figures 4c and 4d). Comparing these time-longitude diagrams finds the tropical standing mode of ENSO at the equator (Figure 4c) with nearly twice the amplitude of the GEW (Figure 4b), as observed by *White and Cayan* [2000], with the peak standing mode anomalies of 0.5 hPa and peak GEW anomalies of 0.3 hPa. However, in the Southern Ocean at 56°S (Figure 4f) the PSA pattern displays an amplitude 1/2–1/3 that of the ACW (Figure 4e), with the peak standing mode anomalies of 0.8 hPa and peak ACW anomalies of 2.4 hPa. Thus removing the tropical standing mode of ENSO from the SLP anomalies over the globe does not improve visualization of eastward propagation in the ACW (Figure 4e), but it significantly improves visualizing of eastward propagation in the GEW (Figure 4b). With the tropical standing mode removed, the GEW can be seen propagating across the Indo-Pacific Ocean with nearly uniform amplitude of 0.1 to 0.3 hPa, decreasing only as it propagates into the Atlantic Ocean.

[17] The tropical standing mode of ENSO on the equator (Figure 4c) and at 56°S (Figure 4f) have similarities; that is, both are characterized by global zonal wave number 2, in agreement with Figures 1 and 2. In the eastern Pacific basin near 90°W, along the vertical dashed line in Figure 4, the tropical standing mode of ENSO in the eastern equatorial Pacific Ocean (Figure 4c) is directly out of phase with the PSA in the eastern Pacific sector of the Southern Ocean at 56°S (Figure 4f). This is consistent with the observation that the PSA and the tropical standing mode of ENSO are linked through meridional atmosphere teleconnections [*Cai and Baines*, 2001] (see Figure 1). Yet at 56°S the amplitude of the ACW is 2 to 3 times larger than that of the PSA, indicating that the ACW cannot possibly be remotely forced by the PSA. This conclusion is supported by the fact that the ACW and the PSA at 56°S (Figures 4e and 4f) are not in phase near 90°W.

[18] On the other hand, note that the speed of eastward phase propagation of the GEW in the Warm Pool (Figure 4b), given by the gradient of the sloping black line extending from 90°E to 150°W (in degrees longitude per year), is the same as that of the ACW in the eastern Pacific and western Atlantic sectors of the Southern Ocean at 56°S, given by the gradient of the sloping black line extending from 150°W to 30°W (Figure 4e). This suggests that the GEW in the Warm Pool remotely forces the ACW in the eastern Pacific and western Atlantic sectors of the Southern Ocean through meridional atmosphere teleconnections (see below). This hypothesis is made more credible since the amplitude of the ACW increases monotonically as it propagates eastward across the eastern Pacific and western Atlantic sectors of the Southern Ocean from 150°W to 30°W, suggesting that it is being forced continuously as it propagates; that is, it is in ''damped resonance'' with the remote forcing [e.g., *Zwillinger*, 1996, p. 424].

## 6. Atmospheric Teleconnection Linking the GEW to the ACW

[19] Results in Figure 4 suggest that eastward phase propagation of the GEW in the Warm Pool reinforces the ACW in the eastern Pacific and Atlantic sectors of the Southern Ocean remotely via fast atmospheric teleconnections. This occurs if we can show warm (cool) SST anomalies in the GEW exciting positive (negative) D200 anomalies overhead in the tropics, the latter driving poleward (equatorward) anomalous Hadley Cells and poleward (equatorward) DV200 anomalies, both of which are capable of initiating quasi-stationary Rossby waves in the background upper level Westerly Winds [*Sardeshmukh and Hoskins*, 1988]. Two key questions must be answered: Do the anomalous Hadley Cells and the anomalous DV200 propagate slowly eastward with the GEW, and do they force the ACW over its entire path or only in the vicinity of the Warm Pool?

[20] We begin answering these questions by computing the extended empirical orthogonal function (EEOF) analysis [*Weare and Nasstrom*, 1982] of modified interannual ST, SLP, D200, DU200, and DV200 anomalies from 1982 to 1999. The tropical standing mode of ENSO is suppressed in these modified interannual anomalies (see section 2). We begin by displaying the dominant EEOF modes of the ST, SLP, and D200 anomalies in Figure 5a, explaining 47%, 47%, and 48% of the total modified interannual variance, respectively. The spatial lag sequences (Figure 5b) are modulated by time sequences of amplitudes (Figure 5a), which correlate significantly with one another without the EEOF of the three variables being computed jointly, indicating that they covary naturally. The lag sequences (Figure 5b) display the eastward phase propagation of covarying ST, SLP, and D200 signals in the GEW, with positive (negative)

**Figure 3.** (opposite) Animation sequences of maps for modified interannual SLP and ST anomalies extending over 10 years from January 1983 to January 1993. Each map in the animation sequence extends zonally around the globe in the latitude band from 20°N to 70°S. Interannual anomalies have been band-pass filtered in time for periods ranging from 3 to 6 years over the 18 years from 1982 to 1999; then the interannual Niño-3 SST index was regressed against each record, and that portion related to the tropical standing mode of ENSO was removed (see section 2). Individual maps are 6 months apart. The sense of propagation comes from following anomalies of similar sign from one map to the next in each time sequence. Yellow-to-red (blue) colors indicate positive (negative) anomalies, with contours at intervals of 0.1°C and 0.4 hPa.

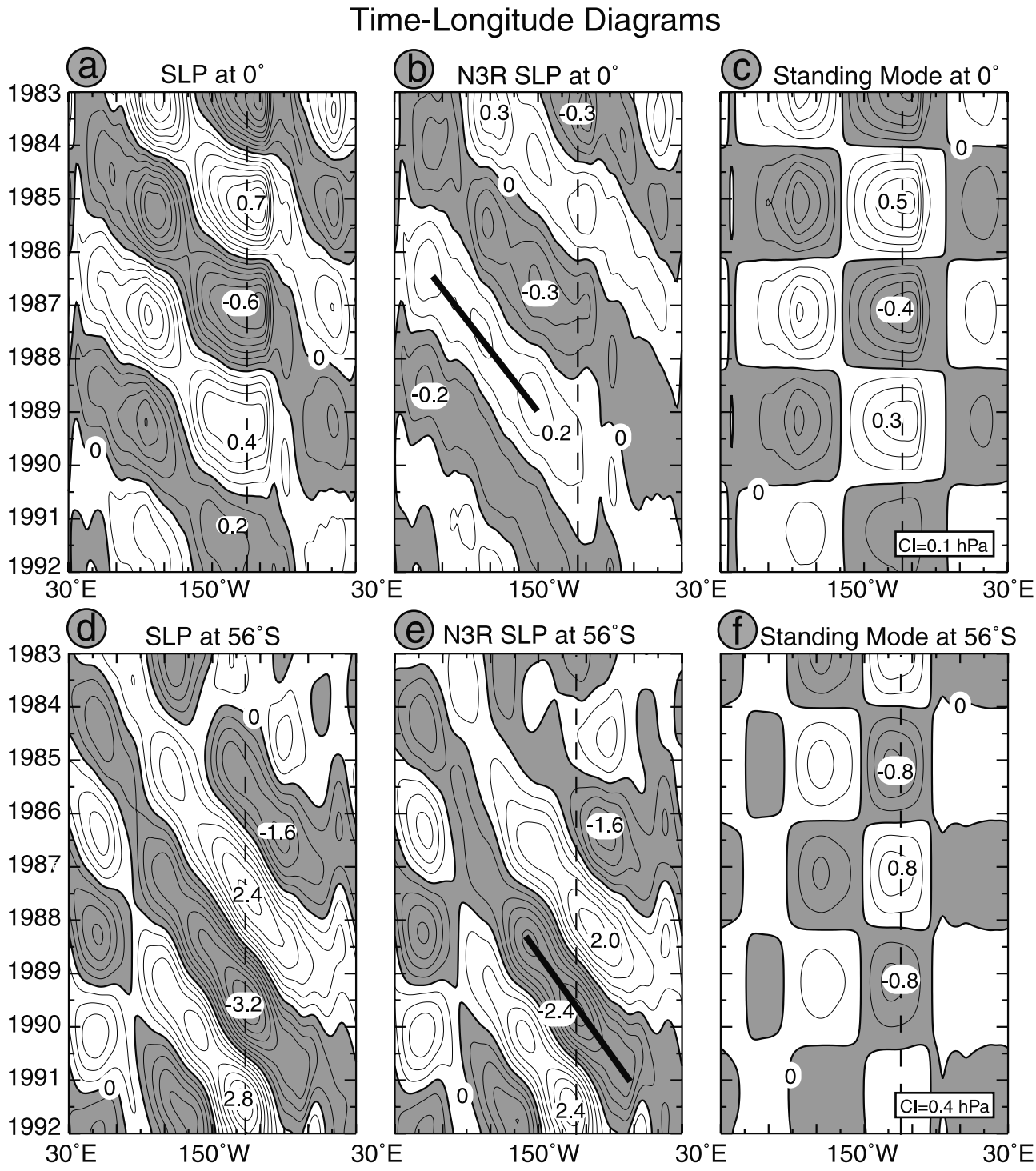


**Figure 4.** (a) Time-longitude diagrams of interannual SLP anomalies along the equator extending around the globe over the 10 years from 1983 to 1992, band-pass filtered for periods ranging from 3 to 6 years over 18 years from 1983 to 1992. (b) Time-longitude diagrams of interannual SLP anomalies modified by regressing the interannual Niño-3 SST index against each record and removing that portion related to the tropical standing mode of ENSO (see section 2). (c) Time-longitude diagrams for the difference between Figures 4a and 4b, showing the tropical standing mode of ENSO in SLP along the equator Negative (positive) anomalies are shaded (unshaded). (d) Same as Figure 4a except at 56°S. (e) Same as Figure 4b except at 56°S. (f) Same as Figure 4c except at 56°S.

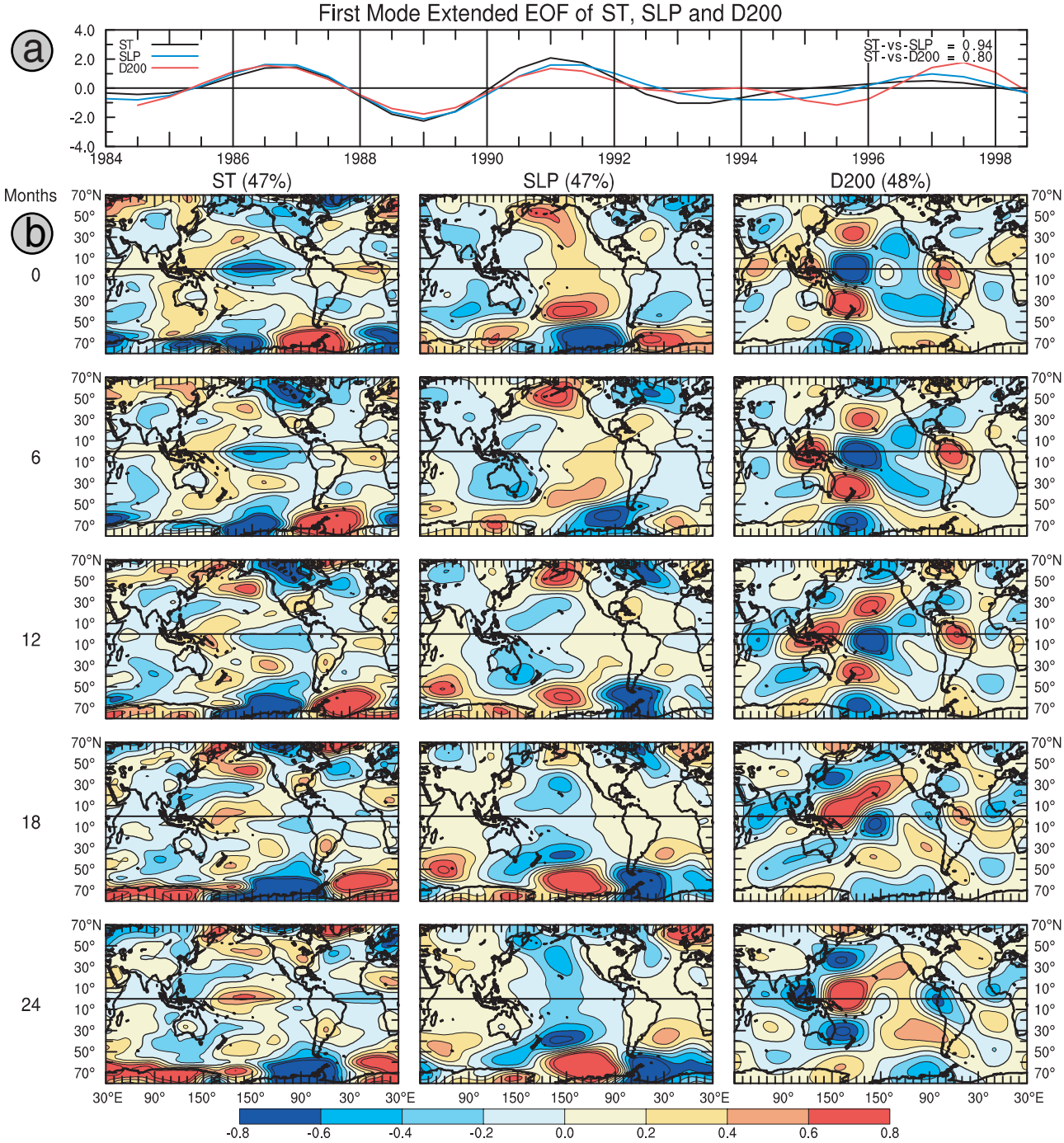


**Figure 5.** (a) Time sequences of amplitudes associated with the dominant EEOF modes of modified interannual ST, SLP, and D200 anomalies for the 18-year record from 1984 to 1999. Time sequences of ST and SLP (ST and D200) correlate at 0.94 (0.80), significant at the 95% confidence level for ~10 effective degrees of freedom [*Snedecor and Cochran*, 1980]. (b) Lag sequences of maps associated with the dominant EEOF modes of interannual SST, SLP, and D200 anomalies, with each map extending over the global ocean zonally from 70°N to 80°S. Each lag sequence extends over 24 lag months, or ~1/2 cycle of variability. Positive (negative) SST, SLP, and D200 weights are colored yellow to red (light blue to dark blue), yielding phase and relative magnitude. Contour intervals for spatial weights of all three variables are given by the color bar in units of standard deviation, with temporal amplitudes also given in units of standard deviation.

D200 weights in the Warm Pool located directly over warm (cool) SST weights on the equator, with corresponding negative (positive) D200 weights located directly poleward near 30°S, representing tropical and subtropical limbs of the anomalous Hadley Cells, respectively. Thus eastward phase propagation of the GEW along the equator, observed by following covarying ST, SLP, and D200 weights eastward from lag 0 to lag 24, can be seen extending its influence to 30°S via this anomalous Hadley Cell activity. These anomalous Hadley Cells are most intense emanating from the Warm Pool extending from 90°E to 150°W; outside this longitude domain the subtropical limbs of the anomalous Hadley Cells are relatively weak.

[21] *Sardeshmukh and Hoskins* [1988] found DV200 anomalies capable of generating quasi-stationary Rossby waves in the background upper level Westerly Winds through the anomalous advection of the mean absolute vorticity gradient. To establish the presence of this mechanism, we superimpose the EEOF lag sequences of the D200 anomalies and the vectors of DU200 and DV200 anomalies for lag months 0, 12, and 24 (Figure 6). This overlay demonstrates that positive D200 weights in the GEW along the equator in the Warm Pool (i.e., 90°E to 150°W) are associated with vectors of divergent wind weights which loop poleward to negative D200 weights in the subtropics (i.e., the subtropical limb of the anomalous Hadley Cell) but also extend to negative D200 weights at higher latitudes near 60°S, only to return to the equator at other negative D200 weights both east and west. The longitudes where these vector divergent wind weights are normal to the background upper level Westerly Winds near 35°S, a potential source of quasi-stationary Rossby waves is indicated, as occurs in lag month 0 (Figure 6a) near 90°E and 120°W and at lag month 12 (Figure 6b) near 60°E, 150°E, 140°W. On the other hand, because the upper level Westerly Winds are most intense off the east coast of Australia from 150°E to 180°, this longitude domain is expected by *Sardeshmukh and Hoskins* [1988] to be the dominant source for quasi-stationary Rossby waves deriving from divergent wind anomalies. We examine this issue below.

[22] On the equator, DU200 weights can also be seen driving anomalous Walker Cell activity, connecting positive and negative D200 weights along the equator (Figure 6b). However, DU200 weights can also be seen linking some of the positive and negative D200 weights in the subtropics near 30°S (Figure 6c), indicating the presence of anomalous zonal cells off the equator similar to but weaker than anomalous Walker Cell activity on the equator. This is true as well for DU200 weights linking some of the positive and negative D200 weights at higher southern latitudes near the sea ice edge around Antarctica (Figure 5b). These high-latitude positive (negative) D200 weights also overlie warm (cool) SST anomalies in the ACW (Figure 5b), suggesting that anomalous SST-induced deep convection in the troposphere can also occur in the ACW.

[23] We summarize these results by plotting the geographical distribution of the RMS of modified interannual D200 anomalies, (Figure 7a), and the RMS of modified interannual DV200 anomalies, weighted by the background winter absolute vorticity gradient at 200 hPa (Figure 7b). These variables represent the two dominant forcing terms expected to generate quasi-stationary baroclinic Rossby waves in the upper level Westerly Winds [*Sardeshmukh and Hoskins*, 1988]. Both forcing terms can be seen to achieve similar maximum magnitude south of the Warm Pool near 30°S, between 90°E and 150°W. Outside this longitude domain both forcing terms near 30°S are significantly smaller. This indicates that the propagation of the GEW across the Warm Pool from 90°E to 150°W carries with it both D200 and DV200 anomalies directly south near 30°S (see figures 5 and 6) which force quasi-stationary Rossby waves in the mean upper level Westerly Winds directly. Thus we can expect these waves to force the ACW in the eastern Pacific and western Atlantic sectors of the Southern Ocean as shown by *Sardeshmukh and Hoskins* [1988] and indicated in Figure 4. The large RMS of the weighted D200 anomalies located at the sea ice edge at 60°S directly south of New Zealand and extending eastward across the Amundson and Bellingshausen Seas will not have a significant effect, since they are well south of the maximum in mean upper level Westerly Winds near 30°S [*Peixoto and Oort*, 1992].

## 7. Oceanic Teleconnection Linking the ACW to the GEW

[24] We utilize covariance analysis to construct phase velocities for modified interannual SLP and ST anomalies (Figure 8) on a 5° latitude-longitude grid from 60°S to 60°N over the 10 years from 1983 to 1992 when the ACW and GEW were both robust [*White and Peterson*, 1996; *White and Cayan*, 2000]. The modified interannual anomalies have had the tropical standing mode of ENSO suppressed (see section 2). Zonal and meridional components of phase velocity were determined independently from space-time lag correlation matrices of modified interannual anomalies computed at each grid point. The phase speed for each component is given by the slope of the line drawn from the origin in the space-time lag correlation matrix through the locus of points yielding maximum correlation in time and space lag dimensions [*White et al.*, 1985]. We extended maximum lags to ±45° latitude and ±90° longitude, allowing the decorrelation of global zonal wave number 2 to be captured.

[25] The distribution of phase velocity for SLP anomalies (Figure 8a) shows eastward phase propagation dominating the entire global domain from 60°S to 30°N, with zonal phase speed maximum in the tropics, decreasing poleward because of the spherical shape of the Earth but also because the zonal average phase speed of the GEW in the global tropical ocean (i.e., 60° to 90° longitude per year) is faster than that (i.e., 45° longitude per year) of the ACW in the Southern Ocean (Figure 4). Northward (southward) components of SLP phase velocity yield undulating zonal paths for the GEW across the global tropical ocean and for the ACW in the Southern Ocean, the latter propagating at about half the speed of the former (in m $s^{-1}$) over most of their respective paths. The distribution of phase velocity for ST anomalies (Figure 6b) shows eastward phase speeds dominating most of the global domain from 60°S to 60°N. In this variable we can see the path of the GEW in the tropical global ocean to be distinct from that of the ACW in the Southern Ocean, again the latter propagating at about half the speed of the former.

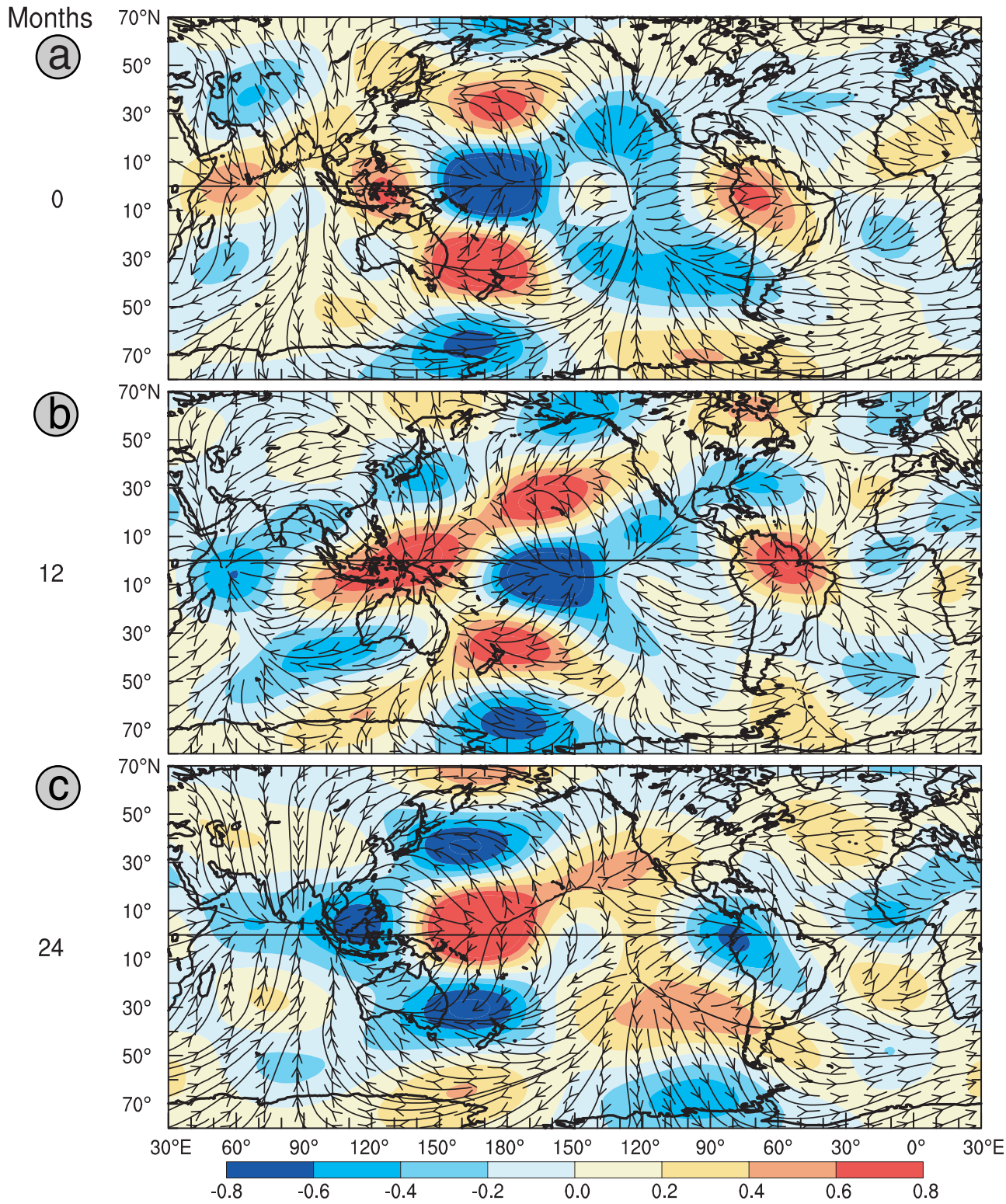


**Figure 6.** EEOF lag sequence of maps associated with the dominant EEOF mode of interannual D200 anomalies from Figure 5, with the vector streamlines from corresponding EEOF lag sequences of DU200 and DV200 anomalies superimposed. Here we display only lag months (a) 0, (b) 12, and (c) 24, extending over ~1/2 cycle of variability. Positive (negative) D200 weights are colored yellow to red (light blue to dark blue), yielding phase and relative magnitude. Contour intervals for spatial weights of D200 are given by the color bar in units of standard deviation, with temporal amplitudes also given in units of standard deviation. The vector streamline weights are also given in units of standard deviation.

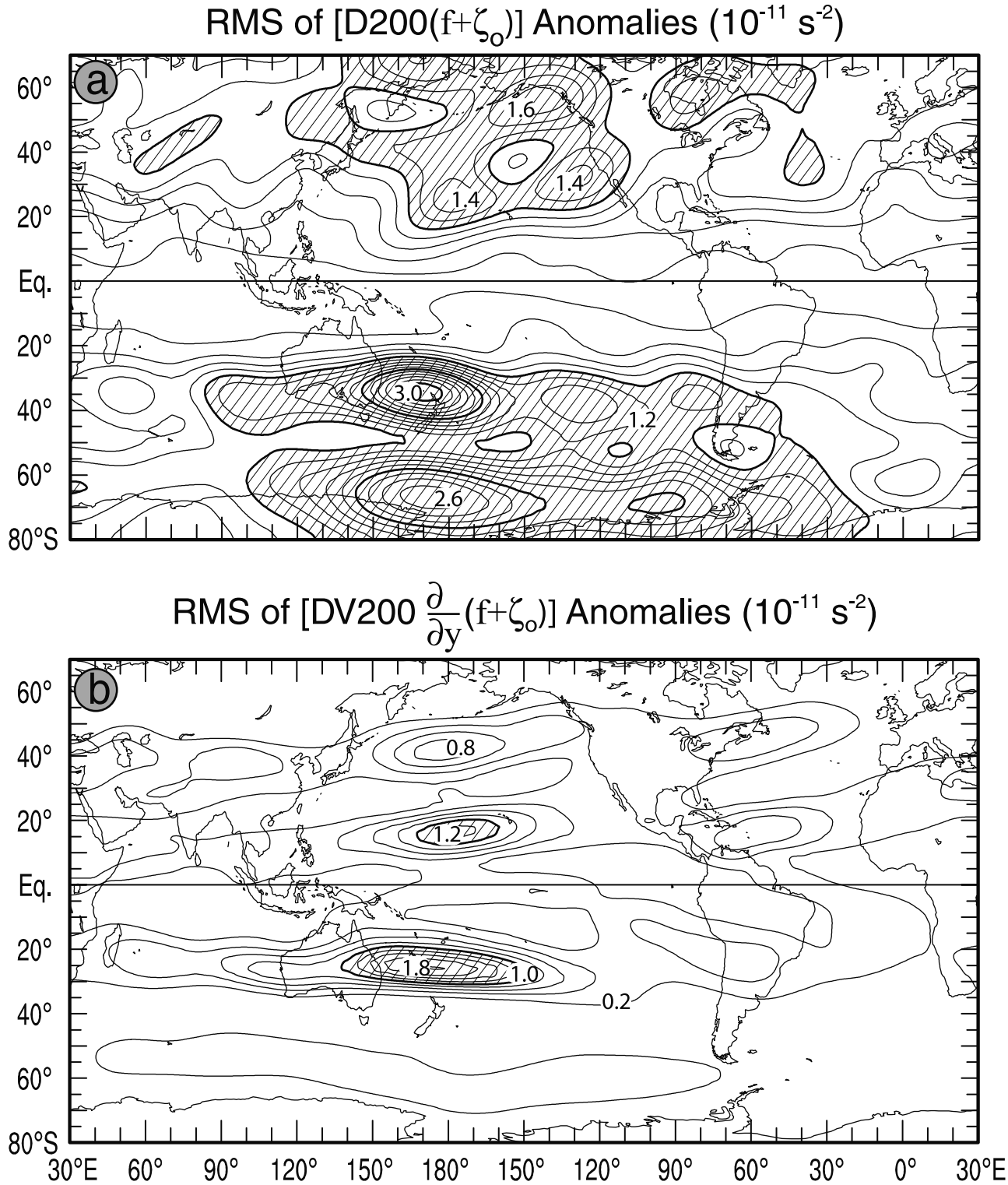


**Figure 7.** (a) The global distribution of the RMS of modified interannual D200 anomalies, weighted by the background absolute vorticity at 200 hPa during winter (JJA) in units of $10^{-11}$ $s^{-2}$, from 70°N to 80°S for the 10 years from 1983 to 1992. (b) The corresponding global distribution of the RMS of modified interannual DV200 anomalies, weighted by the meridional gradient of the background absolute vorticity at 200 hPa during winter (JJA) in units of $10^{-11}$ $s^{-2}$. Shading is for effect. Interannual anomalies used to compute the RMS in both panels were modified by suppressing the tropical standing mode of ENSO (see section 2). The weighting of both variables allows the magnitude of each to be compared to the other when used as forcing terms in the quasi-stationary Rossby wave equation in the winter mean upper level Westerly Winds [*Sardeshmukh and Hoskins*, 1988].

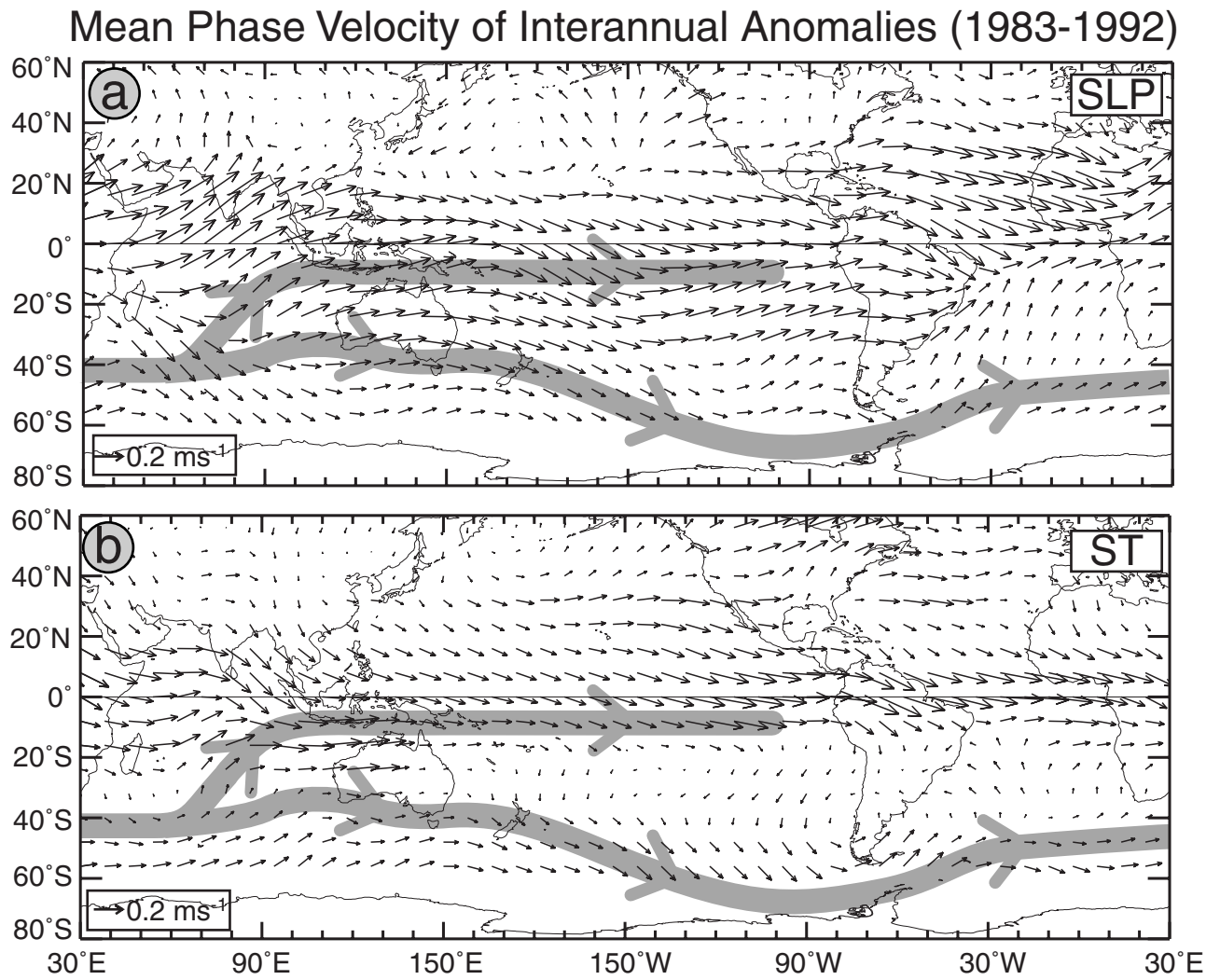


**Figure 8.** Global distributions of the time mean phase velocity for modified interannual (a) SLP and (b) ST anomalies over the global ocean from 60°N to 60°S for the 10 years from 1983 to 1992. Interannual anomalies were modified by suppressing the tropical standing mode of ENSO (see section 2). See text for details on how the phase velocities were computed from the anomalies. Phase speed is proportional to vector length, given in the inset in units of m $s^{-1}$. The thick shaded band circling the Southern Ocean in each map indicates the path along which covarying SLP and ST anomalies in the ACW propagate eastward around the globe. The northern extension of this path from the Indian sector of the Southern Ocean into the Warm Pool south of Indonesia, and eastward across the tropical Indo-Pacific Ocean at 10°S, indicates the path along which ST anomalies in the ACW propagate northward through the Indian Ocean, interfering with the zonal path of the GEW in the tropics along which covarying SLP and ST anomalies propagate eastward across the Warm Pool into the tropical Pacific Ocean.

[26] Zonal phase speeds of the GEW in SLP and ST anomalies in the tropical global ocean are similar, ranging from 0.20 to 0.30 m $s^{-1}$, while zonal phase speeds of the ACW in covarying SLP and ST anomalies in the Southern Ocean are also similar, ranging from 0.05 to 0.15 m $s^{-1}$. Thus the ACW propagates eastward at 1/6 to 3/4 the celerity of the GEW depending on geographical location. The fact that local SLP and ST anomalies propagate with similar zonal phase speeds is consistent with the coupling dynamics between the ocean and atmosphere believed to be responsible for both the GEW and the ACW. Coupling dynamics of the ACW have been examined by *Jacobs and Mitchell* [1996], *Qiu and Jin* [1997], *White et al.* [1998], *Talley* [1999], and *Baines and Cai* [2000], while those for the global ENSO wave have been examined by *Tourre and White* [1997] and *White and Cayan* [2000]. In each case, coupling wave dynamics are considered to be local (not global), with both tropical and extratropical waves following paths along which the coupling can both maintain the signal and propagate it to the east.

[27] *Peterson and White* [1998] and *White* [2000] observed the north branch of the ACW propagating equatorward from the Indian sector of the Southern Ocean into the Warm Pool south of Indonesia following the path of northeastward geostrophic-plus-Ekman surface current from south of Madagascar into the eastern tropical Indian Ocean north of Australia.

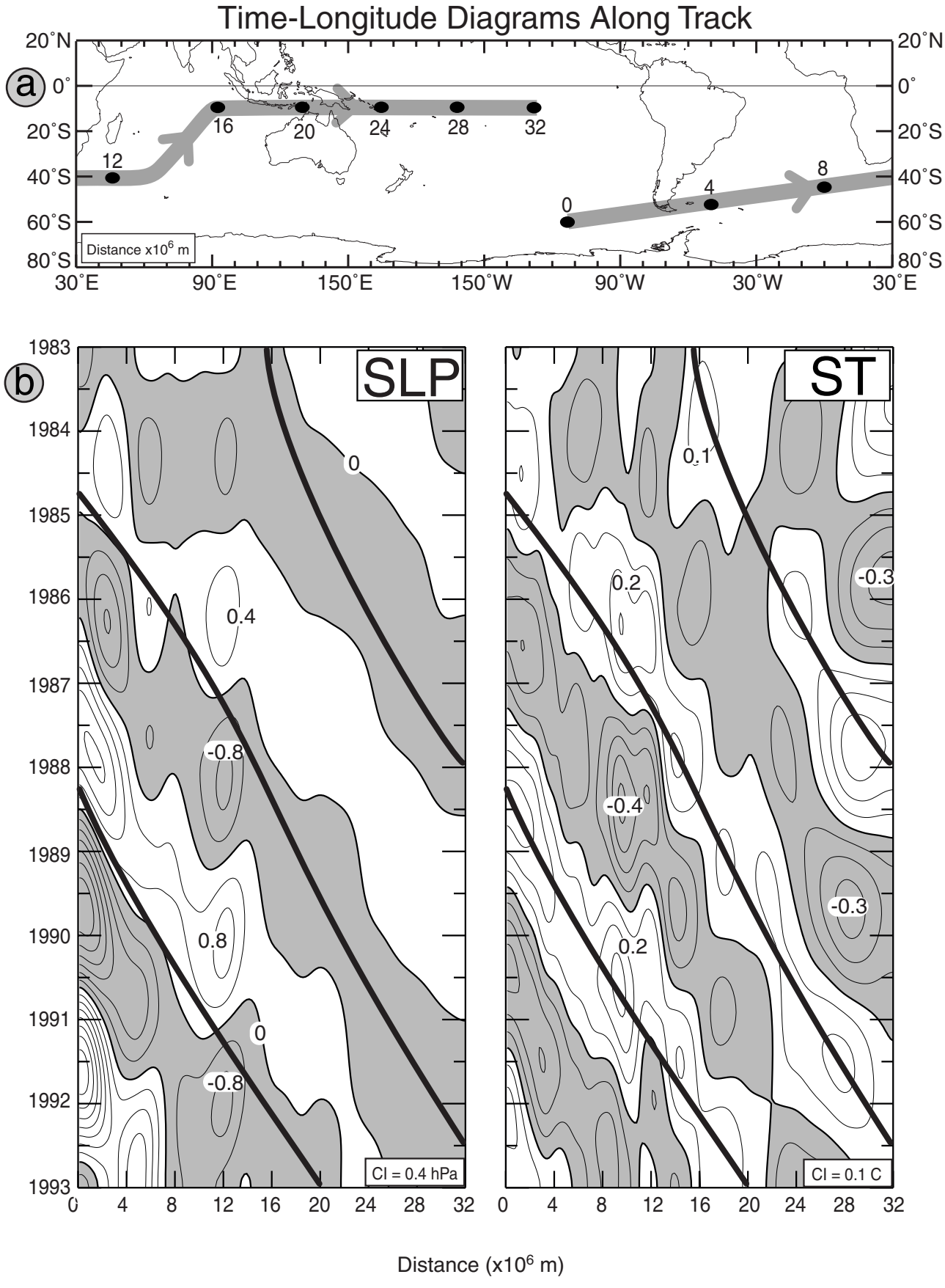

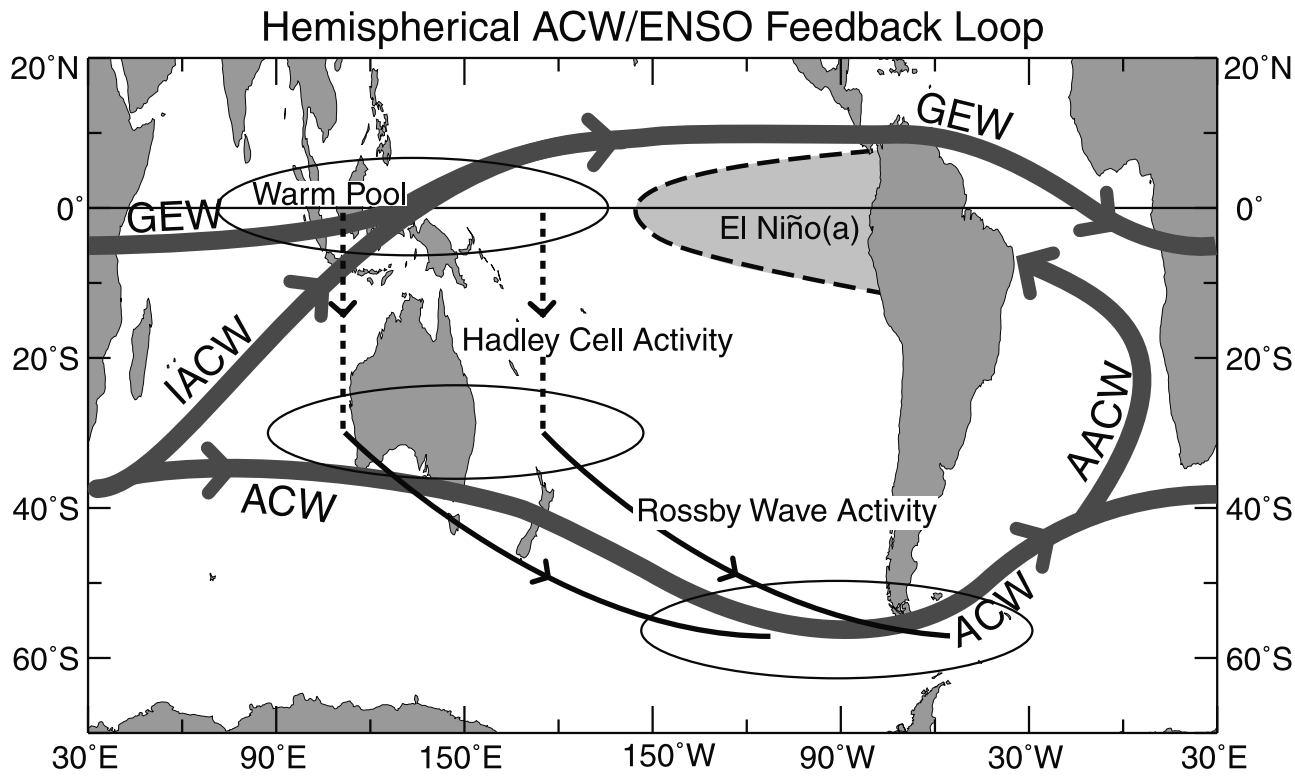


**Figure 10.** Cartoon showing the hemispheric circuit linking the ACW in the Southern Ocean and the GEW in the global tropical ocean. The thick shaded band in the tropics delineates the path of the GEW as it propagates eastward around the global tropical ocean, influencing the phase and amplitude of El Niño/La Niña as it passes the central and eastern tropical Pacific Ocean. A thick shaded band in the Southern Ocean delineates the path of the ACW propagating eastward around the globe, including the north branch into the tropical Atlantic Ocean (AACW) and the north branch into the eastern tropical Indian Ocean (IACW). The latter interferes constructively with the GEW in the vicinity of the Warm Pool near Indonesia. Subsequently, the GEW transits the Warm Pool, where it in turn reinforces the ACW in the eastern Pacific and western Atlantic sectors of the Southern Ocean through atmospheric teleconnections, which propagate eastward along with it. The latter occur as the GEW transits the Warm Pool from 90°E to 150°W, instigating anomalous Hadley cell activity and anomalous DV200, both of which force a quasi-stationary Rossby wave train in winter mean upper level Westerly Winds, forcing the ACW in the eastern Pacific and western Atlantic sectors of the Southern Ocean from 150°W to 30°W along the great circle route [*Sardeshmukh and Hoskins*, 1988].

However, *Peterson and White* [1998] were unable to trace this north branch of the ACW into the western tropical Pacific Ocean. By suppressing the influence from the tropical standing mode of ENSO, we can now see this connection between the ACW and the GEW in the global distribution of phase velocity, with equatorward phase propagation in the Indian Ocean of ST anomalies (Figure 8b), as well as eastward phase propagation from the tropical Indian Ocean into the tropical Pacific Ocean near 10°S.

[28] To confirm the influence of the ACW upon the GEW, we trace a path through the Southern Hemisphere oceans (Figure 9a) beginning in the eastern Pacific sector of the Southern Ocean where the GEW reinforces the ACW, extending eastward into the Indian sector of the Southern Ocean, then equatorward into the tropical Warm Pool, and eastward again along 10°S into the eastern tropical Pacific Ocean. Time-distance diagrams of modified interannual SLP and ST anomalies (Figure 9b) along this path are displayed for 10 years from 1983 to 1992. In the eastern Pacific, Atlantic, and western Indian sectors of the Southern Ocean from 0 to 12 along the path (Figure 9a), covarying SLP and ST anomalies of the ACW can be seen propagating eastward, with high SLP

**Figure 9.** (opposite) (a) The path of the ACW signal emanating from eastern Pacific sector of the Southern Ocean (designated 0) and following the thick shaded band in Figure 8 into the Indian sector of the Southern Ocean (designated 12) where it spawns the north branch of the ACW propagating equatorward into the tropical Warm Pool southwest of Indonesia (designated 16) and eastward into the central tropical Pacific Ocean along 10°S (designated 32). (b) Time-distance diagrams of modified interannual SLP and ST anomalies over the 10 years from 1983 to 1992. Interannual anomalies were modified by suppressing the tropical standing mode of ENSO (see section 2). Negative (positive) anomalies are shaded (unshaded). Black sloping lines in the two panels are synchronous in time and space, allowing the SLP and ST anomalies in both diagrams to be aligned, and the gradient of which yields the phase speed along the track.

anomalies displaced ~90° of phase to the east of warm SST anomalies, as observed by *White and Peterson* [1996]. In the tropical Indo-Pacific Ocean from 16 to 32 along the path (Figure 9a), high (low) SLP anomalies can be seen overlaying cool (warm) SST anomalies as observed by *White and Cayan* [2000]. The phase speed of propagation along the path is indicated by the gradient of sloping black line (Figure 9b), slower over the Southern Ocean (i.e., ~0.08 m $s^{-1}$) from 0 to 12 along the path, slower still over the Indian Ocean from 12 to 20 along the path (i.e., ~0.04 m $s^{-1}$), and faster over the tropical Pacific Ocean from 20 to 32 along the path (i.e., ~0.20 m $s^{-1}$), fairly consistent with phase speeds displayed in Figure 8.

[29] The continuity of propagation by covarying SLP and ST anomalies along the path (Figure 9a) from the eastern Pacific sector of the Southern Ocean to the tropical Indo-Pacific Ocean through the South Indian Ocean (Figure 9b) indicates that ACW reinforces the GEW in tropical Warm Pool, which continues to propagate eastward across the tropical Pacific Ocean, where *White and Cayan* [2000] find it influencing the amplitude and phase of the Niño-3 SST and SLP indices.

## 8. Discussion and Conclusions

[30] A recent study by *Cai and Baines* [2001] proposed that the ACW in the eastern Pacific sector of the Southern Ocean is forced by the PSA pattern in SLP anomaly, the latter remotely forced by the tropical standing mode of ENSO through fast atmospheric teleconnections [*Hoskins and Karoly*, 1981; *Karoly*, 1989; *Sardeshmukh and Hoskins*, 1988]. Also, *Yuan and Martinson* [2000] found the ACW in sea ice extent (SIE) around Antarctica phase locked to ENSO, arguing that the ACW could not exist in the absence of the tropical standing mode of ENSO.

[31] We set out to test these two assertions by differentiating the ACW from the projection of the tropical standing mode of ENSO into the Southern Ocean. We regress the interannual Niño-3 SST index against interannual SLP and ST anomalies over the globe, recovering the PSA in SLP anomaly in the eastern Pacific and western Atlantic sectors, finding it driven by the tropical standing mode of ENSO as observed by *Cai and Baines* [2001]. However, we find the amplitude of the PSA to be weak compared to that of the ACW, the latter as much as 3 times larger than the former in SLP anomaly. This is also true of the projection of the tropical standing mode of ENSO onto SLP anomalies over the remainder of the Southern Ocean, weaker even than in the PSA. There, correlations between the Niño-3 SST index and local ST and SLP anomalies do not indicate cause and effect via atmosphere teleconnections; rather, they represent a coincidence between the ACW and the tropical standing mode of ENSO. This work yields two major results; first, the ACW exists independently of the tropical standing mode of ENSO, contrary to the opposite view proposed by *Yuan and Martinson* [2000], and, second, the ACW is not pumped by the PSA pattern of SLP anomaly in the eastern Pacific and Atlantic sectors of the Southern Ocean as proposed by *Cai and Baines* [2001].

[32] On the other hand, we do find the ACW in the eastern Pacific and western Atlantic sectors of the Southern Ocean phase locked to the GEW via fast atmospheric teleconnections propagating with the GEW as it transits the tropical Warm Pool from 90°E to 150°W. The GEW, like the ACW, propagates slowly eastward in covarying SLP and ST anomalies, taking 4 to 6 years to transit the global tropical ocean [*White and Cayan*, 2000]. The zonal average phase speed of the GEW is 60° to 90° longitude per year, 1.5 to 2 times faster than the zonal average speed of 45° longitude per year for the ACW in the Southern Ocean [*White and Peterson*, 1996]. Yet we find the GEW slowing down from its global average speed as it cross the Warm Pool from 90°E to 150°W, and we find the ACW speeding up as it crosses the eastern Pacific and western Atlantic sectors of the Southern Ocean from 150°W to 30°W, both speeds matching.

[33] To explain the connection, we find warm (cool) ST anomalies in the GEW driving divergent (convergent) D200 anomalies at the top of the troposphere as the GEW transits the Warm Pool in the tropical Indo-Pacific Ocean. The latter producing anomalous poleward (equatorward) Hadley Cells and poleward (equatorward) DV200 anomalies, both of which extend the influence of the GEW to 30° latitude in both hemispheres. The convergent (divergent) D200 anomalies at the subtropical limb of these anomalous Hadley Cells and the anomalous poleward (equatorward) advection of the mean absolute vorticity by the DV200 anomalies near 30°S are both found capable of forcing quasi-stationary Rossby waves in the winter mean upper level Westerly Winds [*Sardeshmukh and Hoskins*, 1988]. Furthermore, we find the subtropical limb of the anomalous Hadley Cell activity largest south of the Warm Pool from 90°E to 150°W, weak outside this domain, and we find the anomalous advection of the mean absolute vorticity by the DV200 anomalies largest over this same region as well, Thus, as the GEW propagates eastward across the Indo-Pacific Ocean, its ability to excite quasi-stationary Rossby waves in the upper level Westerly Winds is restricted to its transit across the Warm Pool from 90°E to 150°W. Since quasi-stationary Rossby waves propagate into the Southern Ocean along great circle routes [*Hoskins and Karoly*, 1981], their effect on the Southern Ocean is restricted to the eastern Pacific and western Atlantic sectors from 150°W to 30°W, as diagramed schematically in Figure 10.

[34] Thus eastward phase propagation of the GEW across the Warm Pool and of the ACW across the eastern Pacific and western Atlantic sector of the Southern Ocean are observed to be in phase with one another, traveling at the same zonal phase speed (in degrees longitude per year), and are linked by atmospheric teleconnections, with the amplitude of the ACW increasing along its path. All this indicates that the ACW in this longitude domain is in "damped resonance" with remote forcing by the GEW as the latter transits the Warm Pool in the tropical Indo-Pacific Ocean. The "damped resonance" phenomenon is described in standard differential equation textbooks [e.g., *Zwillinger*, 1996, p. 424], with the source of damping (or dissipation) remaining to be determined. Even so, the combination of forcing and dissipation allows the amplitude of the ACW to grow slowly as it crosses the eastern Pacific and western Atlantic sectors of the Southern Ocean, as observed.

[35] This atmospheric teleconnection tells only half the story in the interaction of the ACW and the GEW. The GEW reinforces the ACW in the eastern Pacific and western

Atlantic sectors of the Southern Ocean; subsequently, the ACW propagates this imposed GEW signal throughout the remainder of the Southern Ocean as a coupled wave in covarying ST and SLP anomalies. When the ACW reaches the Indian sector 1.5 to 2.5 years later, it spawns a northern branch, which takes another 1.5 to 2.5 years to propagate the ACW signal equatorward into the Warm Pool south of Indonesia. Here it interferes constructively with the GEW propagating eastward around the global tropical ocean. We can find no interruption in the continuity of covarying SLP and ST anomalies in the ACW as they propagate northeastward through the Indian Ocean into the Warm Pool and join with covarying SLP and ST anomalies in the GEW propagating eastward across the tropical Indo-Pacific Ocean. This indicates that the ACW, which receives positive reinforcement from the GEW in the eastern Pacific and western Atlantic sectors of the Southern Ocean via atmospheric teleconnections, exerts a positive feedback on the GEW via the north branch of the ACW in the Indian Ocean 3 to 5 years later. Thus, from a quasiperiodic point of view, both the ACW and the GEW appear to be continually and contemporaneously reinforcing each other on the same timescale as their 3- to 5-year period scale. This scenario is summarized in the cartoon given in Figure 10.

[36] Earlier, *Cai and Baines* [2001] argued that unless the tropical standing mode of ENSO is robust, the ACW cannot be generated. Here we propose a variation on this theme. We argue that unless the GEW is robust as it transits the Warm Pool, the ACW will not be robust. The question remains whether the ACW can exist on its own without this remote forcing by the GEW, or whether, in the absence of the GEW, the north branch of the ACW through the South Indian Ocean provides a sufficiently large eastward propagating signal in covarying ST and SLP anomalies across the Warm Pool to remotely force that portion of the ACW in the eastern Pacific and western Atlantic sectors of the Southern Ocean. Here we find the ACW interfering constructively with the GEW in the Warm Pool, but it remains to be determined whether this reinforcement is required for the GEW to continue its eastward propagation across the Warm Pool. Sorting out these interactions and feedbacks will require numerical experiments to be conducted with coupled models capable of simulating the tropical standing mode of ENSO, the GEW, and the ACW.

[37] **Acknowledgments.** Appreciation is extended to Arthur (Ted) Walker and Jeffrey Annis who as programmers were responsible for the analyses conducted in this study. We extend our thanks to Andrea Fincham who is responsible for drafting the figures. Warren White is supported by Office of Global Programs of NOAA (NOAA NA 47GP0188-MOD3) at the Experimental Climate Prediction Center. He is also supported by the National Aeronautics and Space Administration (NASA) under contract NA27GPO-539. Warren White is also supported by the National Science Foundation under contract OCE-9910730 and the Scripps Institution of Oceanography of the University of California, San Diego.

## References

Allan, R. J., ENSO and climatic variability in the last 150 years, in *El Niño and the Southern Oscillation*: *Multiscale Variability, Global and Regional Impacts*, edited by H. F. Diaz and V. Markgraf, 496 pp., Cambridge Univ. Press, New York, 2000.

Andersen, N., On the calculation of filter coefficients for maximum entropy spectral analysis, *Geophysics*, *39*, 69–72, 1974.

Baines, P. G., and W. Cai, Analysis of an interactive instability mechanism for the Antarctic Circumpolar Wave, *J. Clim.*, *13*, 127–140, 2000.

Cai, W., and P. G. Baines, Forcing of the Antarctic Circumpolar Wave by El Niño-Southern Oscillation teleconnections, *J. Geophys. Res.*, *106*, 9019–9038, 2001.

Carleton, A. M., Antarctic sea-ice relationships with indices of the atmospheric circulation of the Southern Hemisphere, *Clim. Dyn.*, *3*, 207–220, 1989.

Graham, N. E., and T. P. Barnett, Sea surface temperature, surface wind divergence, and convection over tropical oceans, *Science*, *238*, 657–659, 1987.

Hoskins, B. J., and D. Karoly, The steady linear response of a spherical atmosphere to thermal and orographic forcing, *J. Atmos. Sci.*, *38*, 1179–1196, 1981.

Jacobs, G. A., and J. L. Mitchell, Ocean circulation variations associated with the Antarctic Circumpolar Wave, *Geophys. Res. Lett.*, *23*, 2947–2950, 1996.

Kalnay, E., et al., The NCEP/NCAR 40-year reanalysis project, *Bull. Am. Meteorol. Soc.*, *77*, 437–471, 1996.

Karoly, D. J., Southern Hemisphere circulation features associated with El Niño-Southern Oscillation events, *J. Clim.*, *2*, 11,239–11,252, 1989.

Kaylor, R. E., Filtering and decimation of digital time series, *Tech Rep. Note BN 850*, 14 pp., Inst. of Phys. Sci. and Technol., U. of Md., College Park, 1977.

Peixoto, J. P., and A. H. Oort, *Physics of Climate*, 520 pp., Am. Inst. of Phys., College Park, Md., 1992.

Peterson, R., and W. B. White, Slow oceanic teleconnections linking the Antarctic Circumpolar Wave with the tropical El Niño-Southern Oscillation, *J. Geophys. Res.*, *103*, 24,573–24,583, 1998.

Qiu, B., and F.-F. Jin, Antarctic Circumpolar Wave: An indication of ocean-atmosphere coupling in the extratropics, *Geophys. Res. Lett.*, *24*, 2585–2588, 1997.

Reynolds, R. W., and D. C. Marsico, An improved real-time global sea surface temperature analysis, *J. Clim.*, *6*, 114–119, 1993.

Sardeshmukh, P. D., and B. J. Hoskins, The generation of global rotational flow by idealized tropical divergence, *J. Atmos. Sci.*, *45*, 1228–1251, 1988.

Slutz, R. J., S. J. Lubker, J. D. Hiscox, S. D. Woodruff, R. L. Jenne, D. H. Joseph, P. M. Steurer, and J. D. Elms, *Comprehensive Ocean-Atmosphere Data Set, Release 1*, 268 pp., NOAA Environ. Res. Lab., Boulder, Colo., 1985.

Snedecor, G. W., and W. G. Cochran, Statistical Methods, 507 pp., Iowa State Press, U. Ames, 1980.

Talley, L. D., Simple coupled midlatitude coupled models, *J. Phys. Oceanogr.*, *29*, 2016–2037, 1999.

Tourre, Y., and W. B. White, Evolution of the ENSO signal over the Indo-Pacific domain, *J. Phys. Oceanogr.*, *27*, 683–696, 1997.

Weare, B., and J. Nasstrom, Examples of extended empirical orthogonal function analysis, *Mon. Weather Rev.*, *110*, 481–485, 1982.

Webster, P. J., The role of hydrological processes in ocean-atmosphere interactions, *Rev. Geophys.*, *32*, 427–476, 1994.

White, W. B., Influence of the Antarctic Circumpolar Wave upon Australia precipitation from 1958 to 1996, *J. Clim.*, *13*, 2125–2141, 2000.

White, W. B., Evidence for coupled Rossby waves in the annual cycle of the Indo-Pacific Ocean, *J. Phys. Oceanogr.*, *31*, 2944–2957, 2001.

White, W. B., and D. R. Cayan, A global El Niño-Southern Oscillation wave in surface temperature and pressure and its interdecadal modulation from 1900 to 1997, *J. Geophys. Res.*, *105*, 11,223–11,242, 2000.

White, W. B., and R. Peterson, An Antarctic Circumpolar Wave in surface pressure, wind, temperature, and sea ice extent, *Nature*, *380*, 699–702, 1996.

White, W. B., G. Meyers, J. R. Donguy, and S. E. Pazan, Short-term climate variability in the thermal structure of the Pacific Ocean during 1979–1982, *J. Phys. Oceanogr.*, *15*, 917–935, 1985.

White, W. B., S.-C. Chen, and R. Peterson, The Antarctic Circumpolar Wave: A beta-effect in ocean-atmosphere coupling over the Southern Ocean, *J. Phys. Oceanogr.*, *28*, 2345–2361, 1998.

Yuan, S., and D. G. Martinson, Antarctic sea ice variability and its global connectivity, *J. Clim.*, *13*, 1697–1717, 2000.

Zwillinger, D., *Standard Mathematical Tables and Formulae*, 30th ed., 812 pp., CRC Press, Boca Raton, Fla., 1996.

R. J. Allan, Hadley Center for Climate Prediction and Research, Bracknell, Berkshire, RG12 254, UK. (rjallan@meto.gov.uk)

S.-C. Chen and W. B. White, Scripps Institution of Oceanography, La Jolla, CA 92093-0230, USA. (schen@ucsd.edu; wbwhite@ucsd.edu)

R. C. Stone, Queensland Centre for Climate Applications, Department of Primary Industries, 203 Tor Street, Toowoomba QLD 4350, Australia. (stoner@dpi.qld.gov.au)